International Journal of Fluid Machinery and Systems
Vol. 2, No. 1, January-March 2009

Original Paper

Effect of Internal Flow in Symmetric and Asymmetric Micro Regenerative Pump Impellers on Their Pressure Performance

Hironori Horiguchi [1], Shinji Matsumoto [2], Yoshinobu Tsujimoto [1]
Masaaki Sakagami [3] and Shigeo Tanaka [3]

[1] Graduate School of Engineering Science, Osaka University
1-3 Machikaneyama, Toyonaka, Osaka, 560-8531, Japan
[2] ANA Airframe Maintenance Center, All Nippon Airways Co., Ltd.
3-5-4 Haneda Airport, Ota-ku, Tokyo, 144-0041, Japan
[3] Taisei Kogyo Co., Ltd.
26-1 Ikedakita, Neyagawa, Osaka, 572-0073, Japan

Abstract

The effect of symmetric and asymmetric micro regenerative pump impellers on their pressure performance was studied. The shut off head of the pump with the symmetric impeller was about 2.5 times as that with the asymmetric impeller. The computation of the internal flow was performed to clarify the cause of the increase of the head. It was found that the contribution of the angular momentum supply was larger than that of shear stress for the head development in both cases. The larger head and momentum supply in the case of the symmetric impeller were caused by larger recirculated flow rate and larger angular momentum difference between the inlet and outlet to the impeller. The larger recirculated flow rate was caused by smaller pressure gradient in the direction of recirculated flow. The decrease of the circumferential velocity in the casing was attributed to the smaller local flow rate in the casing.

Keywords: Regenerative Pump, Pump Performance, Internal Flow, Leakage Flow, Geometry

1. Introduction

Micro pumps with high discharge pressure are demanded in the fields of micro, bio, and chemical applications and energy-related devices such as micro heat exchangers. Practical applications of micro pumps are also expected for medical devices such as portable fluid delivery systems and for fuel supply to fuel cells. Regenerative pumps have desirable characters with high discharge pressure and continuous discharge unlike positive-displacement type fluid machinery. Consequently, the development of the micro regenerative pump with the impeller whose diameter is about 10mm has been carried out in our research group.

In the prototype of micro regenerative pump made by our research group, a single sided impeller was chosen for the easiness of manufacturing. By a computation of the internal flow, it was found that the discharge pressure increased when the side clearance between the impeller and the casing was decreased due to the decrease of the leakage flow. From this result, it is expected that the leakage flow is decreased and the discharge pressure is increased if the vanes are attached in both sides of the impeller.

In the present study, a capability of the increase of discharge pressure by using a symmetrical impeller with vanes on both sides was investigated. The influence of an internal flow to the discharge pressure was also examined by computation.

2. Experimental Setup and Experiment

The schematic of the regenerative pump with a symmetrical impeller and the coordinate system are shown in Fig.1. Figure 2 shows the cross section of the pump. The materials of the impeller and the casing are aluminum and transparent acrylic resin, respectively. The values of the parameters shown in Figs.1 and 2 are given in Table 1. For the accurate adjustment of the clearance between the impeller and the casing, which would largely affect the performance, the size of the pump is increased to about ten times of the targeted micro regenerative pump. The thickness of the vane is 5 mm so that it is not extremely thin in real micro regenerative pump. The diameter of the impeller D_T is 75mm and the axial clearance c_1 between the impeller and the casing is 1.2mm. This value is pretty large as compared with industrial pump but might be required when manufacturing the micro pump

Received September 8 2008; accepted for publication January 28 2009: Review conducted by Prof. Hyung Hee Cho. (Paper number O08026)
Corresponding author: Hironori Horiguchi, Associate Professor, horiguti@me.es.osaka-u.ac.jp

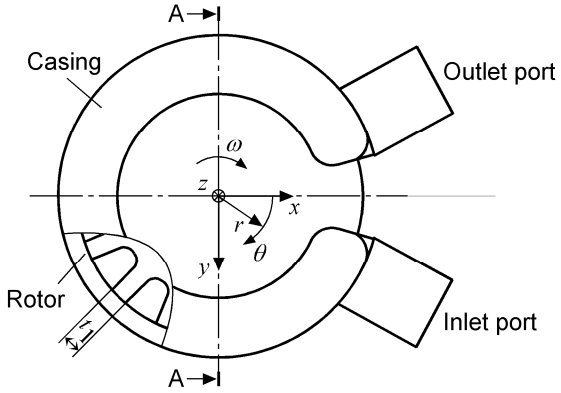

Fig. 1 Schematic of the regenerative pump with symmetric impeller

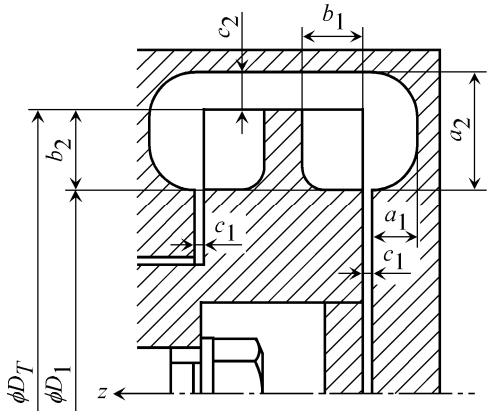

Fig. 2 View of A-A cross section and parameters of the pump with symmetric impeller

Table 1 Dimensions of the test impeller and casing

A: Pump with symmetric impeller
B: Pump with asymmetric impeller

		A	B
Impeller	Number of vanes, Z	16	〃
	Diameter, D_T (mm)	75.0	83.0
	Diameter, D_1 (mm)	54.0	←
	Vane width, t_1 (mm)	5.0	←
	Groove depth, b_1 (mm)	8.0	←
	Groove length, b_2 (mm)	10.5	13.5
Casing	Channel depth, a_1 (mm)	6.0	←
	Channel width, a_2 (mm)	15.5	←
Clearance	Front clearance, c_1 (mm)	1.2	←
	Side clearance, c_2 (mm)	5.0	1.0

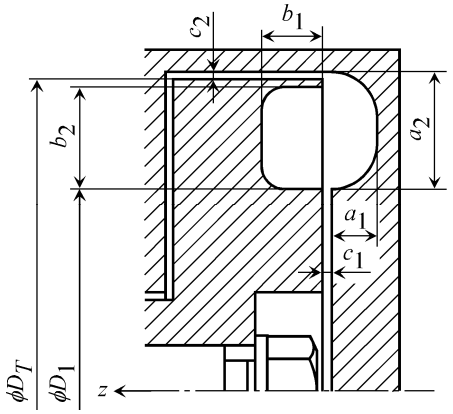

Fig. 3 Meridional plane and parameters of the pump with asymmetric impeller

with 1/10 size. The larger thickness of the vanes and the larger clearance are different from conventional regenerative pumps. The depth of the casing flow path a_1 and the depth of the vane channel b_1 are 6mm and 8mm, respectively. These values were selected to realize the highest head based on preliminary tests with asymmetric impellers. The meridional cross-section and the dimensions of the pump with the asymmetric impeller are shown in Fig.3 and Table 1. The geometry of the casing for the symmetric impeller is made by setting the casing for the asymmetric impeller symmetrically to the z direction. The geometry of the symmetric impeller is produced by back-to-back setting the asymmetric impeller and cutting the impeller at the diameter of $D_T = 75$ mm. A lot of researches for general regenerative pumps with symmetric impellers have been done to achieve the high performance of pumps [1-4]. In the present study, $D_T = 75$ mm was determined for high discharge pressure following [2].

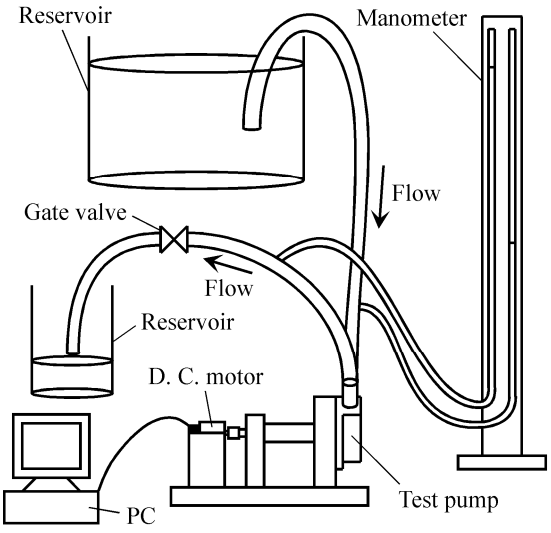

Fig. 4 Experimental setup

Figure 4 shows the schematic of the experimental setup. The impeller is driven by a blushless servomotor. The rotational speed is 600rpm. The flow rate is adjusted by controlling the downstream valve and estimated by measuring the weight of discharged fluid. The pressure coefficient ψ is estimated from the pressures at the wall of the inlet pipe about 9.4 times of the casing diameter (85mm) upstream from the shaft axis and at the wall of the outlet pipe about 11.8 times of the casing diameter downstream from the shaft axis. The working fluid is a water with ambient temperatures (about 25 degrees Celsius). The Reynolds numbers defined by the impeller diameter D_T and the tip speed U_T are about 2.0×10^5 and 2.4×10^5 for the pumps with the symmetric and asymmetric impellers, respectively. These values are about 10 times of the Reynolds number for the targeted micro pump.

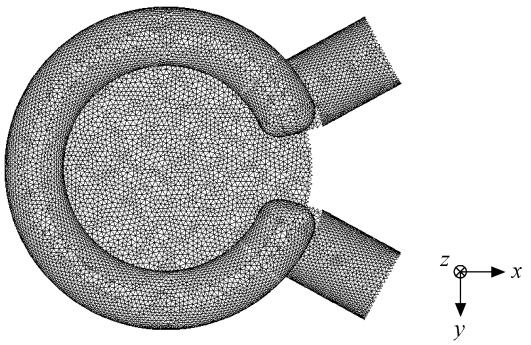

Fig. 5 Computational grid on the casing surface

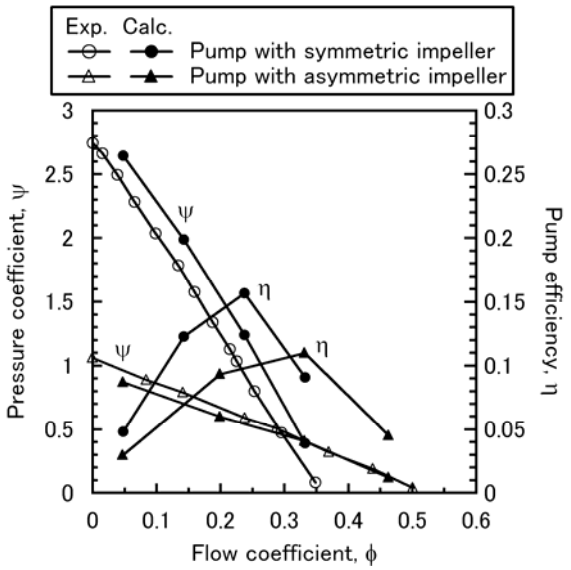

Fig. 6 Performance curve

3. Computation

For the analysis of the internal flow, a commercial software ANSYS CFX-10.0 was used. Basic equations are the continuity equation and the Reynolds averaged Navier-Stokes equation. SST turbulence model are used.

The computational domain consists of the rotational domain of the impeller, the static domains of the casing, the inlet and outlet pipes. The computational grid on the casing is shown in Fig.5. The geometry of the computational cells is mainly tetrahedral and triangular prism near the wall. The impeller rotates around the *z* axis shown in Fig.1. The center lines of the inlet and outlet pipes are at $\theta = -28.6\,\mathrm{deg}$ and 28.6deg, respectively. The lengths of the inlet and outlet pipes are about 11.1 and 13.5 times of the casing diameter (only a part is shown in Fig.5). The number of the computational cells for the pump with the symmetric impeller is about 310 thousands in the impeller, about 740 thousands in the casing, about 60 thousands in the inlet pipe, about 70 thousands in the outlet pipes, and about 1,170 thousands in total. The number of the computational cells for the pump with the asymmetric impeller is about 220 thousands in the impeller, about 430 thousands in the casing, about 50 thousands in the inlet pipe, about 60 thousands in the outlet pipes, and about 760 thousands in total. To confirm the accuracy in evaluating the leakage flow, calculations for the pump with the asymmetric impeller were made with 6 and 12 computational cells in the clearance c_1 between the impeller and the casing. The difference of the values of the pressure coefficient ψ in the both calculations was less than 0.1%. In the present study, 6 cells were used in the clearance c_1 to reduce computational load.

The static pressure at the inlet, the mass flow rate at the outlet, and a non-slip condition on the wall were given as boundary conditions. Unsteady calculation was performed. The time step is 1/400 of one period of the rotation of the impeller. The results shown in the present study are the results at least after 3 revolutions of the impeller where the fluctuation of the head becomes periodic. Working fluid is water with ambient temperatures (25 degrees Celsius).

4. Results and Discussions

4.1 Performance Curve

Figure 6 shows the performance curves from experiments and computations. The effect of changing the asymmetric geometries of the impeller and the casing into the symmetrical ones are significant and the value of the pressure coefficient ψ of the pump with the symmetric impeller at the shutoff flow rate ϕ=0 is about 2.5 times as large as that of the pump with the asymmetric impeller.

The value of the pressure coefficient ψ obtained by the computation is not in good agreement with the experimental results, but similar to them qualitatively. The cause of the quantitative disagreement is not clear.

Figure 6 also shows the pump efficiency obtained by the computation. The maximum efficiencies of the pumps with the symmetric and asymmetric impellers are about 16% at ϕ=0.24 and 11% at ϕ=0.33, respectively.

4.2 Angular Momentum

The angular momentum in the casing was investigated to clarify the cause of the large difference of the performance curves. Figure 7 shows control volumes. The control volumes are set in the casing flow passage excluding the inlet and outlet regions ($-45\,\mathrm{deg} < \theta < 45\,\mathrm{deg}$). Surface 1 of the control volume is located at an axial distance of 1.2mm (=c_1) from the side of the impeller vane. Surface 2 of the control volume for the symmetrical impeller is located at a radial distance of 1.0mm from the tip of the impeller.

We consider the conservation law of the angular momentum around the axis of the impeller using the circular cylinder coordinate system shown in Fig.1. Since the temporal change of the angular momentum due to the impeller vane passage is not negligible, we use the unsteady conservation law of the angular momentum.

$$AM^*_{pressure} = -\frac{dL^*}{dt^*} + AM^*_{flux} + AM^*_{shear} \qquad (1)$$

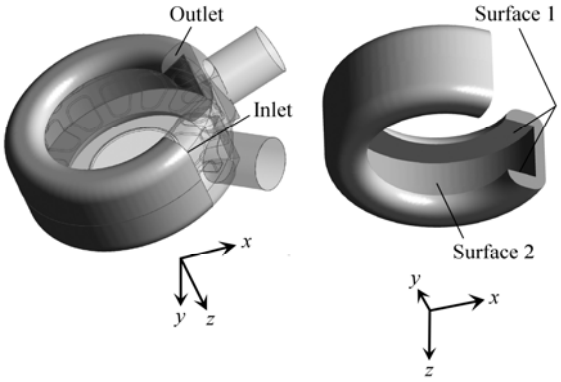

(a) Pump with symmetric impeller

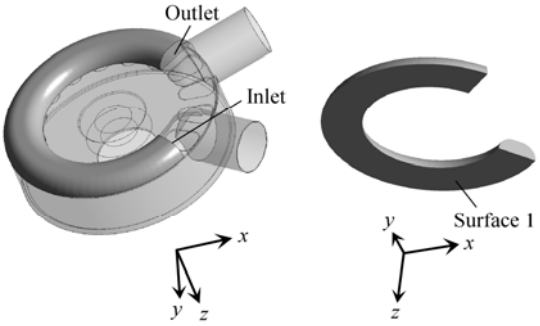

(b) Pump with asymmetric impeller

Fig. 7 Control volumes for the estimation of angular momentum

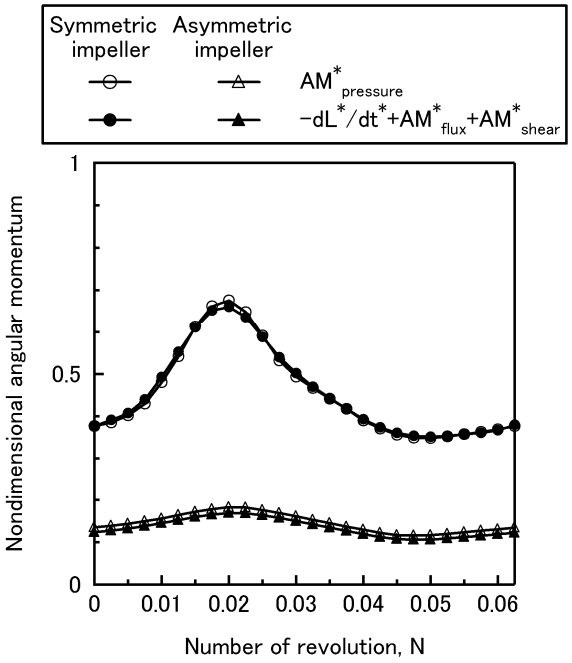

Fig. 8 Conservation of the angular momentum at ϕ=0.047

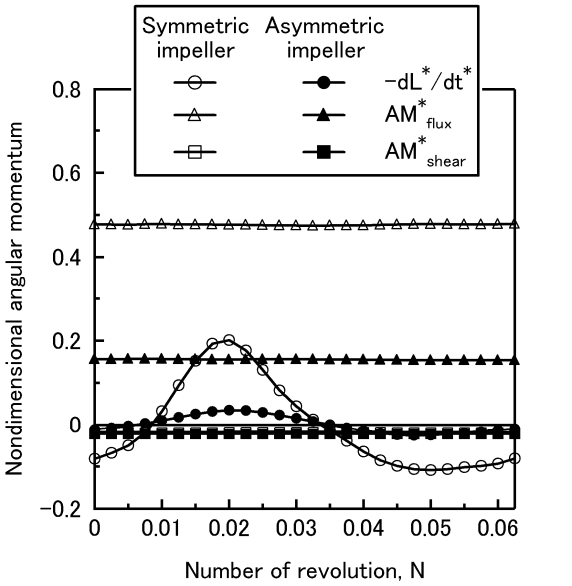

Fig. 9 Components of the angular momentum at ϕ=0.047

where

$$AM^*_{pressure} = \left(\sum_i r_i \cdot \Delta a_{outlet,i} \cdot p_{outlet,i} - \sum_i r_i \cdot \Delta a_{inlet,i} \cdot p_{inlet,i} \right) / \left(\rho A U_T^2 D_T \right)$$

$$L^* = \rho \sum_i \Delta V_i \cdot r_i \cdot v_{\theta,i} / \left(\rho A U_T D_T^2 \right)$$

$$AM^*_{flux} = \left(\sum_i \Delta \dot{m}_{in,i} \cdot r_i \cdot v_{\theta,i} - \sum_i \Delta \dot{m}_{out,i} \cdot r_i \cdot v_{\theta,i} \right) / \left(\rho A U_T^2 D_T \right)$$

$$AM^*_{shear} = T / \left(\rho A U_T^2 D_T \right)$$

$$t^* = t / \left(D_T / U_T \right)$$

$AM^*_{pressure}$ is the moment of the pressure forces at the inlet and outlet boundary. L^* is the angular momentum in the control volume, AM^*_{flux} is the angular momentum of the fluid entering the control volume, AM^*_{shear} is the moment due to the shear force on the surface of the control volume, and t^* is the nondimensional time.

4.3 Effect of Geometry to Angular Momentum

First, we discuss the angular momentum at the low flow rate ϕ=0.047 where the difference of the pressure coefficients ψ of the pumps with the symmetric and asymmetric impellers is larger.

Figure 8 shows the value of $AM^*_{pressure}$ on the left hand side of Eq.(1) and the value of $-dL^*/dt^* + AM^*_{flux} + AM^*_{shear}$ on the right hand side of Eq.(1). The number of vanes is 16 and the value of the angular momentum fluctuates with one sixteenth of the rotational period. Therefore, the results in one sixteenth periods are shown. At the number of revolution of N=0, the center lines of vanes are at θ=45deg and -45deg, i.e., at the inlet and outlet surfaces of the control volume, respectively. The values of $AM^*_{pressure}$ and $-dL^*/dt^* + AM^*_{flux} + AM^*_{shear}$ are nearly equal and the conservation law are satisfied fairly well in both cases of the pumps with the symmetric and asymmetric impellers.

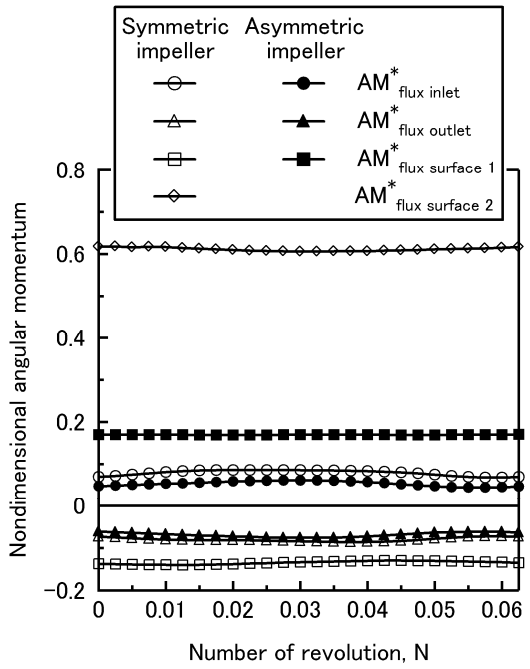

Fig. 10 Angular momentum supplied by the fluxes from the surfaces of the control volume at ϕ=0.047

Table 2 Mass flow rate into/out from the control volume through the surface 1 and 2, and mean circumferential velocity

	Pump with symmetric impeller		
	in	out	out-in
ϕ_c	1.93	1.86	0.07
$\bar{v}_\theta/U_T$	0.72	0.42	0.30

	Pump with asymmetric impeller		
	in	out	out-in
ϕ_c	1.31	1.26	0.05
$\bar{v}_\theta/U_T$	0.67	0.58	0.09

Figure 9 shows the values of $-dL^*/dt^*$, AM^*_{flux} and AM^*_{shear}. It is found that the temporal changes of $AM^*_{pressure}$ are mainly due to $-dL^*/dt^*$. The value of AM^*_{flux} is larger than the average of $-dL^*/dt^*$ and the value of AM^*_{shear} in both pumps.

The averages of $-dL^*/dt^*$ and the values of AM^*_{shear} in both pumps are nearly equal, respectively. The value of AM^*_{flux} of the pump with the symmetric impeller is about 3 times as large as that of the pump with the asymmetric impeller. It is found that the influence of the difference of the pump geometry largely appears in the value of AM^*_{flux}.

4.4 Angular Momentum of the Flow Entering the Control Volume

Figure 10 shows the values of the angular momentum which enters the control volume through each surface. $AM^*_{flux\ inlet}$, $AM^*_{flux\ outlet}$, $AM^*_{flux\ surface1}$ and $AM^*_{flux\ surface2}$ are the angular momenta which flow into the control volume through the inlet and outlet surfaces, and the surfaces near the impeller (Surface 1 and 2) shown in Fig.7, respectively. Absolute values of $AM^*_{flux\ inlet}$ and $AM^*_{flux\ outlet}$ are similar and their signs are opposite. Therefore, $AM^*_{flux\ inlet}$ and $AM^*_{flux\ outlet}$ do not contribute to the pressure rise. $AM^*_{flux\ surface2}$ of the pump with the symmetric impeller and $AM^*_{flux\ surface1}$ of the pump with the asymmetric impeller largely contribute to the pressure rise.

Although the value of $AM^*_{flux\ surface1}$ is negative in the pump with the symmetric impeller, the total angular momentum of $AM^*_{flux\ surface1}$ and $AM^*_{flux\ surface2}$ is larger than $AM^*_{flux\ surface1}$ of the pump with the asymmetric impeller. To clarify the cause of that, a flow rate ϕ_c of the fluid which flows in/out from the control volume through Surface 1 and 2 and its averaged circumferential velocity $\bar{v}_\theta/U_T$ were examined. The results at a number of the revolution of $N=0$ are shown in Table 2. The right column in Table 2 shows the difference of ϕ_c and $\bar{v}_\theta/U_T$ of the inflow and outflow. Although the difference of ϕ_c of the inflow and outflow from Surface 1 and 2 exists, the continuity equation is satisfied if we consider the inflow and outflow from the surfaces of Inlet and Outlet shown in Fig.7. The flow rate ϕ_c of the fluid which goes through the impeller is about 1.9 in the pump with the symmetric impeller and about 1.3 in the pump with the asymmetric impeller.

In the pump with the symmetric impeller, the values of $\bar{v}_\theta/U_T$ of the fluid which flows in and flows out from the control volume are 0.72 and 0.42, respectively, and their difference is 0.30. In the pump with the asymmetric impeller, the values of $\bar{v}_\theta/U_T$ of the fluid which flows in the control volume is 0.67 and similar to that (0.72) of the pump with the symmetric impeller and the values of $\bar{v}_\theta/U_T$ of the fluid which flows out from the control volume is 0.58 and larger than that (0.42) of the pump with the symmetric impeller. The difference of $\bar{v}_\theta/U_T$ of the inflow and outflow is 0.09 and quite small.

From these results, it was found that the higher pressure rise was realized in the pump with the symmetric impeller because the difference of the angular momenta which flow in/out from the control volume is larger than that of the pump with the asymmetric impeller due to the larger flow rate ϕ_c and the larger difference of $\bar{v}_\theta/U_T$ of the inflow and outflow.

4.5 Cause of the Changes of the Flow Rate ϕ_c and the Averaged Circumferential Velocity $\bar{v}_\theta/U_T$

The flow rate ϕ_c is determined so that the pressure rise between the inlet and outlet of the vane channel equals the pressure drop in the casing. Figure 11 shows the pressure and velocity distributions on the meridian plane at θ=191.25deg at a number of the revolution of N=0. The pressure is normalized after subtracting the averaged pressure p_{ave} in the meridian plane of the flow path of the casing from the original pressure. Figures 11(a) and (b) show the results for the pumps with the symmetric and asymmetric impellers, respectively. In the pump with the symmetric impeller, the pressure gradient along the circulating flow is smaller in the casing, as shown in Fig.11(a). In the pump with the asymmetric impeller, the pressure gradient along the circulating flow is larger in the casing, as shown in Fig.11(b). To compensate the higher pressure drop in the casing, the pressure increase is higher for the asymmetric impeller. So, it is difficult to say clearly why the recirculation flow rate is higher for the symmetrical impeller. Figure 12 show the control surfaces to estimate the flow rate of the fluid which goes through the flow path of the casing. The lines indicated by the doubly encircled numbers 1-6 in Fig.12 show the control surfaces. The figures in the upper right of

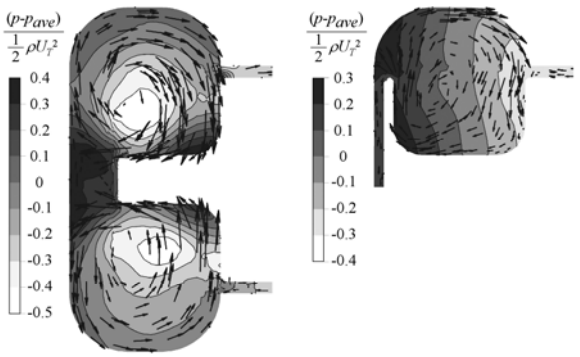

(a)Pump with symmetric impeller (b)Pump with asymmetric impeller

Fig. 11 Pressure distribution and velocity vector on the meridional surface at θ=191.25 deg

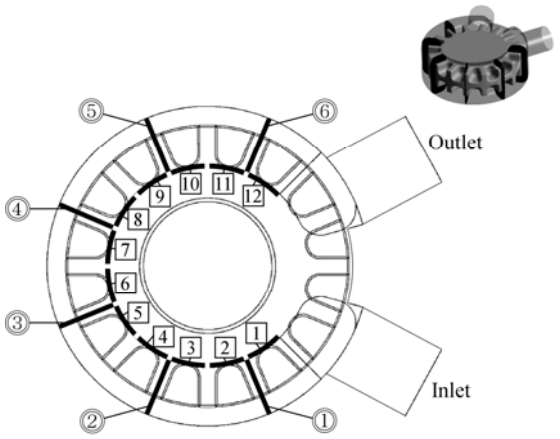

(a) Pump with symmetric impeller

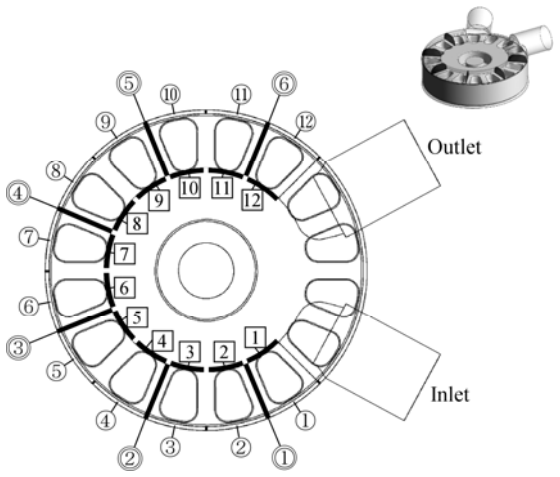

(b) Pump with asymmetric impeller

Fig. 12 Control surface for the local flow rate

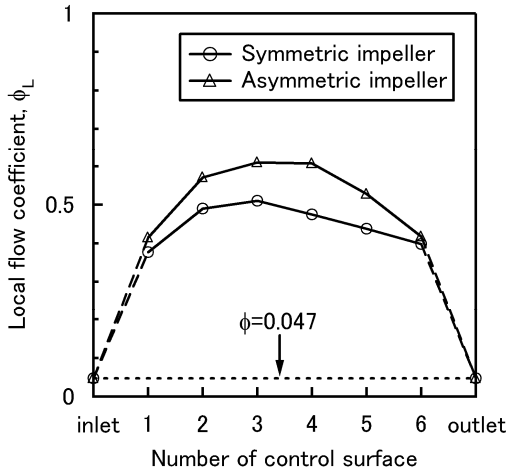

Fig. 13 Local flow rate at ϕ=0.047

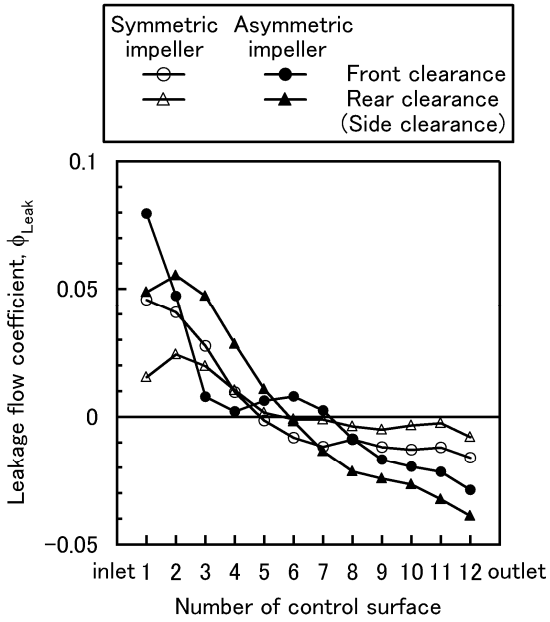

Fig. 14 Local flow rate of leakage flow at ϕ=0.047

Figs.12(a) and (b) also show the control surfaces. Figure 13 shows the local flow rate $\phi_L (= Q/(AU_T) = \overline{v}_\theta / U_T)$ of the fluid which goes through the control surfaces. The value of ϕ_L of the pump with the symmetric impeller is smaller than that of the pump with the asymmetric impeller. The cause of the larger pressure gradient along the circulating flow in the pump with the asymmetric impeller is considered to be a larger centrifugal force in the flow path of the casing due to the larger local flow rate ϕ_L. It is thought that the increase of pressure drop in the casing due to the increase of the centrifugal force causes the decrease of the circulating flow rate ϕ_c in the pump with the asymmetric impeller.

The averaged local flow rates $\overline{\phi}_L$ of the fluid which goes through the control surfaces indicated by the doubly encircled numbers 1-6 in Fig.12 are 0.45 and 0.53 in the pumps with the symmetric and asymmetric impellers, respectively. It is thought that the smaller local flow rate ϕ_L causes the smaller circumferential velocity $\overline{v}_\theta / U_T$ of the fluid which flows out of the control volume in the pump with the symmetric impeller.

The value of the local flow rate ϕ_L is about 10 times as large as the flow rate ϕ=0.047, as shown in Fig.13. To clarify the cause of that, the flow rate through the clearance was investigated. The lines indicated by the numbers 1-12 in squares in Fig.12 show the control surfaces for estimating the flow rate through the clearance. Each control surface has an axial width of 1.2mm, which is the same as the clearance c_1. In the case of the pump with the symmetric impeller, the control surfaces for the clearance are also set in the rear side. In the case of the pump with the asymmetric impeller, the control surfaces indicated by the circled numbers 1-12 are set in the tip clearance of the impeller, as shown in Fig.12(b). The radial width of the control surface in the tip

clearance equals 1.0mm ($=c_2$). The control surface in the tip clearance is located at a distance of 0.5mm to *z* direction from the front surface of the impeller. Figure 14 shows the flow rate ϕ_{Leak} $(=Q_{Leak}/(AU_T))$ of the fluid which goes through the clearance. It was confirmed that the local flow rate ϕ_L is obtained by adding the leakage flow rate ϕ_{Leak} in the upstream to the inlet/outlet flow rate ϕ. It was found that a large amount of fluid flows in/out from the flow path of the casing through the clearance and the increase of the local flow rate ϕ_L from the flow rate ϕ was due to the clearance flow.

The local flow rates ϕ_L and ϕ_{Leak} are defined as the flow rate divided by the area A of the flow path of the casing and the tip speed of the impeller U_T. The area A and the tip speed U_T of the pump with the symmetric impeller are about 3.1 times and about 0.9 times as those of the pump with the asymmetric impeller, respectively. Therefore, the values of ϕ_L and ϕ_{Leak} of the pump with the symmetric impeller should be about one third of those of the pump with asymmetric impeller if the amounts of the leakage flow in both pumps are the same. However, the values of ϕ_L and ϕ_{Leak} of the pump with the symmetric impeller are about 0.85 times as those of the pump with the asymmetric impeller and larger than one third of the values of ϕ_L and ϕ_{Leak} of the pump with the asymmetric impeller. The larger local flow rate ϕ_L of the pump with the symmetric impeller is due to the larger pressure rise.

5. Conclusions

The effect of the internal flow in the symmetric and asymmetric micro regenerative pumps on their pressure performance was investigated in experiments and computations. The following results were obtained.

(1) The pressure coefficient of the pump with the symmetric impeller at the shutoff flow rate was about 2.5 times as large as that of the pump with the asymmetric impeller.
(2) The pressure rise in the pumps is mainly caused by the angular momentum of the fluid which flows in the flow path of the casing from the impeller. This angular momentum is larger and causes the larger pressure rise in the pump with the symmetric impeller.
(3) In the pump with the symmetric impeller, the flow rate of the fluid which flows in the flow path of the casing is larger and the circumferential velocity largely decreases in the flow path of the casing. Therefore, the angular momentum of the fluid which flows in the flow path of the casing is larger.
(4) The cause of the larger flow rate of the fluid which flows in the flow path of the casing in the pump with the symmetric impeller is the smaller pressure gradient along the circulating flow.
(5) The cause of the larger deceleration of the circumferential velocity in the flow path of the casing in the pump with the symmetric impeller is the smaller local flow rate in the flow path of the casing due to the smaller leakage flow rate.

Acknowledgement

This study was financially supported by the Comprehensive Support Programs for Creation of Regional Innovation which is provided by the Japan Science and Technology Agency (JST).

Nomenclature

a_1	Depth of the flow path of the casing [m]	Q_{Leak}	Volume flow rate of the leakage flow through the clearance [m^3/s]
Δa_{inlet}	Minute area on the inlet surface of the control volume [m^2]	r	Radial coordinate
Δa_{outlet}	Minute area on the outlet surface of the control volume [m^2]	t	Time [s]
		t^*	Nondimensional time, Eq.(1)
A	Area in the meridional plane (vane section not included) of the flow path of the casing [m^2]	T	Torque [$N \cdot m$]
		U_T	Tip velocity of the impeller [m/s]
		v_θ	Circumferential velocity [m/s]
AM^*_{flux}	Angular momentum of the fluid which flows in/out from the control volume, Eq.(1)	$\overline{v}_\theta$	Average circumferential velocity [m/s]
		$\Delta \dot{m}_{in}$	Mass flow rate of the fluid which flows in the minute area on the control volume [kg/s]
$AM^*_{flux\ surface1}$, $AM^*_{flux\ surface2}$	Angular momentum of the fluid which flows in/out from the control surfaces near the impeller	$\Delta \dot{m}_{out}$	Mass flow rate of the fluid which flows out from the minute area on the control volume [kg/s]
$AM^*_{pressure}$	Moment generated by a pressure, Eq.(1)		
AM^*_{shear}	Moment generated by a shear force, Eq.(1)	ΔV	Minute volume of the control volume [m^3]
c_1	Axial clearance between the impeller and the casing [m]	ϕ	Flow coefficient $=Q/(AU_T)$
		ϕ_c	Local flow coefficient $=Q_c/(AU_T)$
D_T	Diameter of the impeller [m]	ϕ_L	Local flow coefficient in the flow path of the casing $=Q_L/(AU_T)$
g	Gravity [m/s^2]		
L^*	Nondimensional angular momentum,Eq.(1)	ϕ_{Leak}	Local flow coefficient of the leakage flow $=Q_{Leak}/(AU_T)$
N	Number of the revolution of the impeller		
p_1	Pressure at the inlet [Pa]	η	Pump efficiency $=\phi\psi/(2\tau)$
p_2	Pressure at the outlet [Pa]	θ	Circumferential coordinate

p_{ave}	Average pressure on the meridional plane of the flow path of the casing [Pa]	ρ	Density [kg/m^3]
		τ	Torque coefficient $= T\omega / (\rho A U_T^3)$
Q	Volume flow rate [m^3/s]	ψ	Pressure coefficient
Q_c	Volume flow rate of the fluid which flows in/out from the control volume through the control surfaces near the impeller [m^3/s]		$= (p_2 - p_1) / (\rho U_T^2 / 2)$
		ω	Angular velocity of the impeller
		Subscript	
Q_L	Local volume flow rate through the flow path of the casing [m^3/s]	i	Number of the minute elements at the control volume

References

[1]Wilson, W. A., Santalo, M. A., and Oelrich, J. A., 1955, “A Theory of the Fluid-Dynamic Mechanism of Regenerative Pumps,” Transactions of the ASME, Vol.77, No.8, pp. 1303-1316.

[2]Shimosaka, M. and Yamazaki, S., 1960, “Research on the Characteristics of Regenerative Pump (1st Report, Influence of Flow Channel and Impeller),” Bulletin of JSME, Vol.3, No.10, pp. 185-190.

[3]Yamazaki, S. and Tomita, Y., 1971, “Research on the Performance of the Regenerative Pump with inclined blades (1st Report, Performance and Internal Flow),” Transactions of the Japan Society of Mechanical Engineers, Vol.37, No.295, pp. 506-514 (in Japanese).

[4]Murata, S., Inaba, T., and Hayashi, M., 1980, “An Investigation of Regenerative Fan (1st Report, Influence of Geometries of Impeller and Intake,” Transactions of the JSME, Series B, Vol.46, No.410, pp. 1968-1976 (in Japanese).